

Article

# n\_TOF: Measurements of Key Reactions of Interest to AGB Stars

Cristian Massimi <sup>1,2,\*</sup> , Sergio Cristallo <sup>3,4</sup> , César Domingo-Pardo <sup>5</sup>  and Claudia Lederer-Woods <sup>6</sup><sup>1</sup> Department of Physics and Astronomy, University of Bologna, 40127 Bologna, Italy<sup>2</sup> INFN, Sezione di Bologna, 40127 Bologna, Italy<sup>3</sup> INAF, Osservatorio Astronomico d'Abruzzo, 64100 Teramo, Italy; sergio.cristallo@inaf.it<sup>4</sup> INFN, Sezione di Perugia, 06123 Perugia, Italy<sup>5</sup> Instituto de Física Corpuscular, CSIC—Universidad de Valencia, 46980 Paterna, Spain; domingo@ific.uv.es<sup>6</sup> School of Physics and Astronomy, University of Edinburgh, Edinburgh EH9 3FD, UK;

claudia.lederer@ed.ac.uk

\* Correspondence: cristian.massimi@unibo.it; Tel.: +39-051-2091079

**Abstract:** In the last 20 years, the neutron time-of-flight facility n\_TOF at CERN has been providing relevant data for the astrophysical slow neutron capture process (*s* process). At n\_TOF, neutron-induced radiative capture ( $n,\gamma$ ) as well as ( $n,p$ ) and ( $n,\alpha$ ) reaction cross sections are measured as a function of energy, using the time-of-flight method. Improved detection systems, innovative ideas and collaborations with other neutron facilities have led to a considerable contribution of the n\_TOF collaboration to studying the *s* process in asymptotic giant branch stars. Results have been reported for stable and radioactive samples, i.e.,  $^{24,25,26}\text{Mg}$ ,  $^{26}\text{Al}$ ,  $^{33}\text{S}$ ,  $^{54,57}\text{Fe}$ ,  $^{58,59,62,63}\text{Ni}$ ,  $^{70,72,73}\text{Ge}$ ,  $^{90,91,92,93,94,96}\text{Zr}$ ,  $^{139}\text{La}$ ,  $^{140}\text{Ce}$ ,  $^{147}\text{Pm}$ ,  $^{151}\text{Sm}$ ,  $^{154,155,157}\text{Gd}$ ,  $^{171}\text{Tm}$ ,  $^{186,187,188}\text{Os}$ ,  $^{197}\text{Au}$ ,  $^{203,204}\text{Tl}$ ,  $^{204,206,207}\text{Pb}$  and  $^{209}\text{Bi}$  isotopes, while others are being studied or planned to be studied in the near future. In this contribution, we present an overview of the most successful achievements, and an outlook of future challenging measurements, including ongoing detection system developments.

**Keywords:** *s* process; MACS; time of flight

**Citation:** Massimi, C.; Cristallo, S.; Domingo-Pardo, C.; Lederer-Woods C. n\_TOF: Measurements of Key Reactions of Interest to AGB Stars. *Universe* **2022**, *8*, 100. <https://doi.org/10.3390/universe8020100>

Academic Editor: Lijing Shao

Received: 10 December 2021

Accepted: 28 January 2022

Published: 4 February 2022

**Publisher's Note:** MDPI stays neutral with regard to jurisdictional claims in published maps and institutional affiliations.



**Copyright:** © 2022 by the authors. Licensee MDPI, Basel, Switzerland. This article is an open access article distributed under the terms and conditions of the Creative Commons Attribution (CC BY) license (<https://creativecommons.org/licenses/by/4.0/>).

## 1. Introduction

The slow neutron capture process (the *s* process, see, e.g., [1]) is responsible for forming about half of the elemental abundances heavier than iron. It proceeds via a sequence of neutron captures and  $\beta$ -decays from a seed distribution (around iron), building up elements up to Bi. Except for so-called branching point nuclei (see Section 7),  $\beta$ -decay rates are typically faster than neutron capture rates, which means that reactions proceed along the valley of stability on the chart of nuclei.

The main component of the *s* process is at work during the asymptotic giant branch (AGB) phase of low mass stars ( $1.5 \leq M/M_{\odot} < 4.0$ ) and, to a lower extent, intermediate mass stars ( $4.0 \leq M/M_{\odot} < 7.0$ ). This evolutionary phase consists of a sequence of short convective He-burning runaways (thermal pulses, TPs) interspersed with long periods of quiescent H-burning (interpulses). For reviews on AGB stars, see [2–5]. An additional component to the *s* process, the so-called weak component, is activated during the core He-burning and C-shell burning of massive stars ( $M/M_{\odot} > 10.0$ ) and it largely contributes to abundances between Fe and Zr (see, e.g., [6]).

Together with  $\beta$ -decay rates, neutron capture cross sections represent the basic nuclear physics input to the slow neutron capture process. To a minor extent ( $n,p$ ) and ( $n,\alpha$ ) reactions on a few light elements can play some role as neutron poisons (i.e., these reactions absorb a large number of neutrons, thus affecting the efficiency of the *s* process in synthesizing heavy elements).

Experimentally, ( $n,\gamma$ ) cross section data are typically determined either via two techniques: (i) the activation technique involves a sample first being irradiated with a contin-

uous neutron beam, and subsequently the resulting product nucleus is counted; (ii) the time-of-flight (TOF) technique, relevant for this article, allows the determination of energy-dependent cross sections by inferring the neutron energy from the time of flight of the neutron over a certain flight path length.

Measured cross sections as a function of neutron energy,  $\sigma(E_n)$ , need to be averaged over the thermal energy distribution of neutrons inside AGB stars, before they can be used in stellar models. In fact, the astrophysical reaction rate depends on the number density of interacting particles as well as on the reaction rate per particle pair  $\langle\sigma v\rangle$ . This latter term describes the probability of nuclear reactions between two particles, where  $v$  is the relative velocity. As the interacting particles are in thermodynamic equilibrium in a stellar plasma, their kinetic energy is related to their thermal motion. Consequently, the relative velocity can be described by a Maxwell–Boltzmann distribution  $\phi_{MB}$ <sup>1</sup>. The distribution presents a maximum at the velocity  $v_T = \sqrt{\frac{2kT}{\mu}}$ ; here,  $k$  is the Boltzman constant,  $T$  is the temperature of the stellar environment and  $\mu$  is the reduced mass of the system formed by the interacting particles. The reaction rate per particle pair can then be expressed as:

$$\langle\sigma v\rangle = \int_0^\infty \sigma(v)\phi_{MB}(v)v dv. \tag{1}$$

Typically, neutron-induced reaction cross sections are measured as a function of energy  $E$  (here  $E$  represents the centre-of-mass energy), therefore, it is customary to express the velocity distribution as energy distribution. As a result, Equation (1) becomes:

$$\langle\sigma v\rangle = \left(\frac{8}{\pi\mu}\right)^{1/2} \frac{1}{(kT)^{3/2}} \int_0^\infty E\sigma(E)e^{-\frac{E}{kT}}dE. \tag{2}$$

This reaction rate can be also expressed in terms of the Maxwellian-averaged cross section (MACS):

$$\text{MACS} = \frac{\langle\sigma v\rangle}{v_T} = \frac{2}{\sqrt{\pi}(kT)^2} \int_0^\infty E\sigma(E)e^{-\frac{E}{kT}}dE. \tag{3}$$

Equation (3) clearly shows the advantage of the TOF method, where one obtains energy-dependent cross section data (in contrast to the activation technique). In fact, it is possible to calculate MACSs at all relevant stellar temperatures, which for AGB stars range from  $kT = 8$  keV to  $kT = 30$  keV. Therefore, the  $\sigma(E)$  are required in the epithermal region.

On the other hand, in case of rare and/or short-lived isotopes, it is usually very difficult to produce samples with a sufficient mass (mg or higher) and/or enrichment for a TOF measurement. In these cases, an alternative to TOF measurements is the activation method, provided that neutron captures result in unstable isotopes. The activation technique consists of two different phases: irradiation of the sample under a neutron field and measurement of the capture rate. This latter, derived from the number of freshly produced nuclei, can be measured either through the activity of the sample, for instance using a HPGe detector, or via an AMS measurement [7]. It is important to notice that activation measurements provide a cross section averaged over the neutron spectrum of the used neutron field. Therefore, shaping the neutron spectrum to resemble a Maxwellian spectrum at a certain temperature  $\phi_{MB}(kT)$  makes the measurement of the MACS straightforward.

In Section 2, the features of the n\_TOF facility are presented with a particular focus on the characteristics that make n\_TOF one of the most important facilities for astrophysical studies.

As mentioned above, the experimentally determined MACS are used in stellar models to predict *s*-process isotopic abundances. However, along the reaction flow path,  $(n,\gamma)$  cross sections on certain isotopes can play peculiar roles:

- The main neutron source in low-mass AGB stars is the  $^{13}\text{C}(\alpha,n)^{16}\text{O}$  reaction [8], which releases neutrons in radiative conditions (see, e.g., [9]). The formation of the  $^{13}\text{C}$  reservoir (the so-called  $^{13}\text{C}$ -pocket) needed to reproduce spectroscopic observations and presolar grain measurements is still a matter of debate [10–13]. For this reason, any

source of uncertainty (as its destruction channel via charged particle reactions) has to be reduced as much as possible. The  $^{13}\text{C}$  in the pocket burns radiatively between two TPs at temperatures around 100 MK. However, in some AGB stars it may be engulfed in the next TP, leading to the anomalous production of some isotopes (see, e.g., [14]). A second additional neutron burst is released by the  $^{22}\text{Ne}(\alpha, n)^{25}\text{Mg}$  reaction, which is efficiently activated during TPs at temperatures larger than 300 MK (see, e.g., [15]). Its contribution is particularly important in intermediate mass AGB stars ( $4\text{--}8 M_{\odot}$ ) and in the synthesis of isotopes close to branching points (see item below). The n\_TOF contribution to this topic is discussed in Section 3;

- The seeds for the *s*-process are considered to be the isotopes around the broad iron peak in the Solar System abundance curve ( $^{56}\text{Fe}$  is the most abundant isotope in the upper panel of Figure 1). Those isotopes formed in the last stages of massive star evolution (type II supernovae) and in supernova explosions of type Ia. For nuclei heavier than iron, Coulomb barriers prevent significant synthesis of heavier elements via charged particle reactions, and thus neutron capture reactions are dominantly responsible for their creation. Precise neutron capture cross sections on *s*-process seed isotopes are important, as these impact on the number of neutron captures per seed, which in turn determines in which mass region the peak production of isotopes occurs (for example, a higher neutron capture rate on a seed isotope will lower the number of neutron captures per seed and result in a shift of the peak production to lower mass numbers). This effect is, for example, demonstrated for the case of the  $^{56}\text{Fe}(n, \gamma)$  reaction in Figure 3 of [16]. The n\_TOF contribution to this topic is discussed in Section 4;
- Other interesting isotopes are those with a closed shell configuration. These isotopes, named magic nuclei, are characterized by a very small neutron capture cross section (blue squares in Figure 1). In correspondence to these “nuclear bottlenecks”, the *s* process presents three peaks (see upper panel of Figure 1). Depending on the initial amount of iron seeds, the *s*-process abundance distribution shows different relative enhancements among the three peaks (see, e.g., Figure 18 of [17]). At close-to-solar metallicities, isotopes up to the first peak (Sr–Y–Zr) are favoured, while at lower metallicities, elements belonging to the second peak (Ba–La–Ce) are mostly produced. Finally, at low metallicities, the *s* process may develop up to its termination point (Pb–Bi), where  $^{208}\text{Pb}$  shows the lowest neutron capture cross section (being a double magic nucleus). The n\_TOF contribution to this topic is discussed in Section 5;
- There exist a limited number of isotopes whose production is entirely ascribed to the *s* process: they are known as *s*-only isotopes (magenta triangles in Figure 1). In fact, any contribution from the rapid neutron capture process is shielded by their stable isobars<sup>2</sup>. Those nuclei are almost uniformly distributed along the nuclide chart and are extremely useful to evaluate the robustness of theoretical calculations (see, e.g., [18]). In fact, theoretical stellar models (possibly coupled to galactic chemical evolutionary models) must reproduce the observed distribution of solar *s*-only isotopes at the epoch of the Solar System formation. Local deviations from the observed trends often highlight problems in the adopted nuclear data. The n\_TOF contribution to this topic is discussed in Section 6;
- Along the *s*-process path, there are unstable isotopes where beta decay competes with neutron capture, called branching points. The abundances of the successive isotopes in the reaction flow are sensitive to the branching ratio, which depends on the half-life and the neutron capture cross section at the branching point, and the neutron density in the star. Thus, for branchings which are followed by *s*-only isotopes (i.e., the abundance is well known), the measurement of the neutron capture cross section allows the determination of the neutron density (half lives are usually well-known). If the beta decay half-life is temperature dependent, and the neutron density was already determined from other branchings, the temperature at which *s*-process nucleosynthesis develops can be determined (see, e.g., [19]). The higher

the temperature, the larger the probability to activate these branchings, as neutron densities increase due to higher interaction energies of neutron source reactions. As a consequence, major effects are expected in intermediate mass AGB stars, where temperatures are larger (see, e.g., [20]). In Figure 1, we report the most important branching points of the s process (stable close-by isotopes are magnified with red dots). The n\_TOF contribution to this topic is discussed in Section 7.

- Finally, of extreme interest is any experimental measurement focused on measuring neutron capture cross sections related to processes able to modify the local number of neutrons available to the production of heavy elements.

Apart from the neutron sources already discussed, the neutron density can be modified by so-called neutron poisons. These are light isotopes, which modify the number of neutrons available for the s process, either because of their high abundances, or because their neutron reaction cross sections are comparable to radiative capture on s-process isotopes. The two major neutron poisons in AGB stars are represented by the  $^{14}\text{N}(n,p)^{14}\text{C}$  and the  $^{26}\text{Al}(n,p)^{26}\text{Mg}$  reactions. The n\_TOF contribution to this topic is discussed in Section 8.

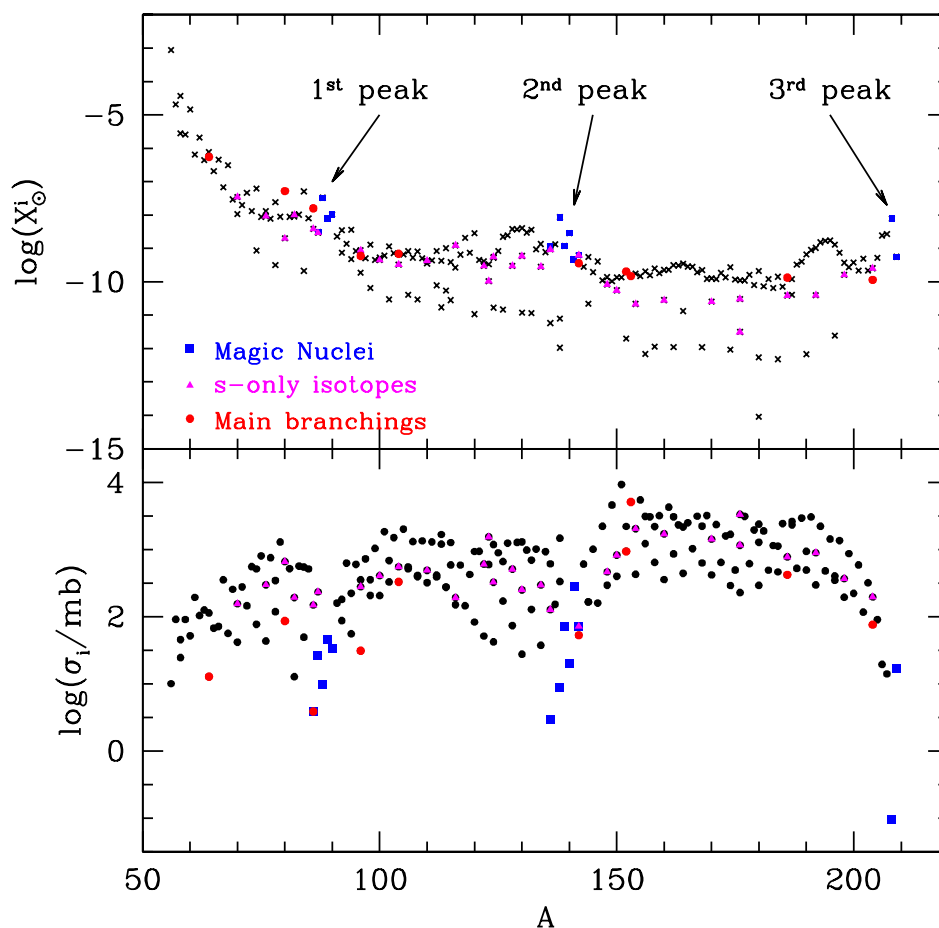


**Figure 1.** Upper panel: isotopic solar distribution (mass fractions); lower panel: isotope neutron capture cross sections (in mb). In each panel, isotopes of interest are magnified (see text for details). The three abundance peaks produced by the s process are highlighted (upper panel).

After this non-exhaustive overview of the n\_TOF contribution to AGB nucleosynthesis, a brief outlook of future perspective is presented in Section 9.

## 2. The n\_TOF Facility at CERN

With the aim of collecting nuclear data of interest for nuclear astrophysics and other applications, the neutron time-of-flight facility n\_TOF [21] was built at CERN some twenty years ago. In the first phase, it consisted of a single beam line positioned at 185 m from the neutron source. Today, after several facility upgrades, two beam lines and corresponding experimental areas EAR1 at 185 m and EAR2 at 19 m are available for TOF measurements. In addition, an irradiation station referred to as NEAR, as well as a measurement station equipped with HPGe detectors for activation measurements, is in construction.

At n\_TOF, neutrons are produced by 20 GeV/c protons from the CERN proton synchrotron (PS) accelerator, impinging onto a massive Pb block, surrounded by a water layer acting as moderator of the initially fast neutron spectrum. This results in a wide neutron energy spectrum at both experimental areas [22,23], ranging from meV to GeV. On the other hand, the high peak current of the PS accelerator, delivering near  $10^{13}$  protons per pulse, results in a very high instantaneous neutron flux. On average,  $5 \times 10^5$  and  $2 \times 10^7$  neutrons per pulse are delivered to EAR1 and EAR2. Their energy distribution is shown in Figure 2.

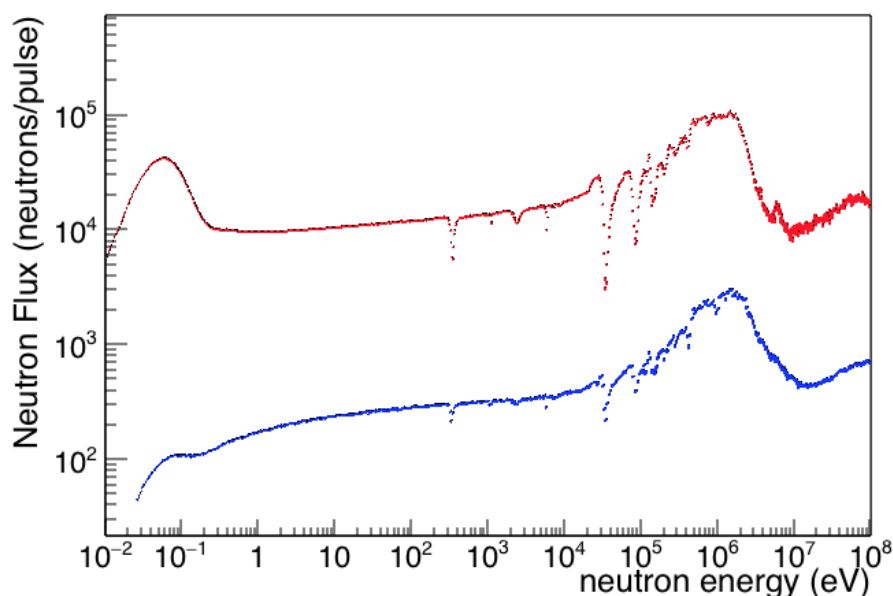


**Figure 2.** Energy distribution of neutrons reaching EAR1 and EAR2 at the sample position. Data from [22,23].

Another important feature is the high resolution in neutron energy (reconstructed from the time of flight). In fact, thanks to the 185 m long flight path and the narrow proton-bunch width of 6 ns RMS, the energy resolution at EAR1 is  $\Delta E/E \approx 10^{-3,-4}$  in the energy region of interest (i.e., in the epithermal region). In fact, when the cross section presents narrow resonances, measurements must be carried out with excellent neutron energy resolution.

Both experimental areas EAR1 and EAR2 are equipped with high-performance detection systems for the detection of  $\gamma$  rays or charged particles, and state-of-the-art data acquisition systems. These include, for instance, a  $4\pi$  total absorption calorimeter made of 40 BaF<sub>2</sub> crystals [24,25] and low-neutron-sensitivity C<sub>6</sub>D<sub>6</sub> detectors [26] optimised by the n\_TOF collaboration for (n, $\gamma$ ) reactions. As a consequence, n\_TOF has allowed us, in some cases for the first time, to measure accurate neutron cross-section data on highly radioactive samples [27–30] and derive MACSs for different stellar temperatures.

After the recent (2020) installation of a new spallation target [31] with a more efficient cooling and ventilation system, an irradiation station (NEAR) was built close to the spallation target. The aim of this new station is to perform activation measurements on short-lived isotopes, taking advantage of the huge neutron fluxes available. In fact, the

possibility to produce rare isotopes at other facilities such as ISOLDE and PSI could lead to fruitful collaborations between these different facilities in the future.

Finally, the n\_TOF project has benefited from the close collaboration with other neutron facilities, in particular GELINA [32], at the European Commission Joint Research Center in Belgium and SARAF [33] in Israel. In fact, several cooperative projects were carried out in order to improve the quality of the cross-section data. One example is related to the measurement of  $^{197}\text{Au}(n,\gamma)$ . This cross section is considered as a reference for neutron flux determination in activation measurements, and therefore it is used to normalise the experimental data and extract Maxwellian-averaged capture cross sections at  $kT = 30$  keV. The n\_TOF and GELINA measurements were prompted by a long-standing debate on the discrepancy between the MACS derived from international evaluations (such as ENDF/B, JEFF, JENDL, ...) and the MACS obtained in two well-known experiments: the activation measurement at the Karlsruhe Van De Graff accelerator by Ratynski and Käppeler [34] and the TOF measurement at Oak Ridge Electron Linear Accelerator (ORELA) by Macklin [35]. The results by these latter experiments were adopted as recommended values for the MACS in the KADoNiS 0.3 database [36], a widely used reference database of stellar neutron capture cross sections for astrophysical studies. Figure 3 shows the MACS obtained at n\_TOF and GELINA compared to the value recommended in KADoNiS 0.3. Clearly, the results of n\_TOF [37,38] and GELINA [39,40] measurements show a 5% deviation in the MACS at  $kT = 30$  keV, confirming values obtained from previous evaluations (ENDF/B, JEFF, JENDL, ...). As a matter of fact, the MACS values of a large number of isotopes that were measured relative to the  $^{197}\text{Au}(n,\gamma)$  cross section have been re-evaluated taking these new data into account [41], and these changes are reflected in the new version of the KADoNiS database KADoNiS 1.0. [42].

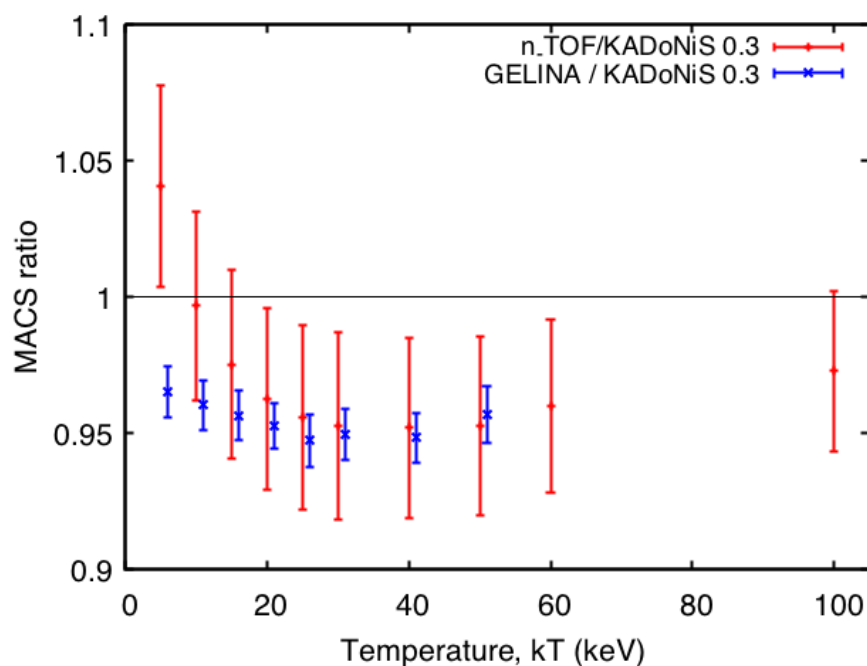


**Figure 3.** Ratio of the  $^{197}\text{Au}(n,\gamma)$  MACSs reported in the KADoNiS 0.3 database with respect to the n\_TOF and GELINA experimental data. To avoid an overlap of points the values corresponding to the GELINA data are displaced along the x-axis by 1 keV.

Other examples are reported in the next sections.

### 3. Stellar Neutron Sources

The difficulties related to the measurement of the cross section of the  $^{13}\text{C}(\alpha,n)^{16}\text{O}$  and  $^{22}\text{Ne}(\alpha,n)^{25}\text{Mg}$  neutron source reactions in the energy region of interest are well known. In

fact, the expected reaction count rate is extremely small and the experimental signature is dominated by background events. Therefore, it is not surprising that a large number of attempts at constraining these cross sections through indirect measurement can be found in the literature, see for instance the recent overviews by Cristallo and collaborators [9] and Adsley and collaborators [15].

By exploiting the principle of time-reversal invariance applied to strong interaction, it is possible to determine the cross section of the  $(\alpha, n)$  reactions by measuring the  $(n, \alpha)$  reaction cross sections. However, the study of the inverse reactions (namely  $^{25}\text{Mg}(n, \alpha)$  and  $^{16}\text{O}(n, \alpha)$ , respectively) are also extremely challenging, and so far only feasibility studies were conducted at n\_TOF. Nevertheless, these cross sections feature structures and resonances, which are related to the excited unbound levels of the compound system formed in the reactions. Consequently, important information, such as the energy and spin parity  $J^\pi$  of the states, can be deduced from neutron-induced reactions. This was the case of the excited levels of  $^{26}\text{Mg}$  above the  $\alpha$  threshold, determined by a joint measurement campaign between n\_TOF and GELINA [43,44].

This study represented an important step forward in the knowledge of low-energy resonances in the  $^{22}\text{Ne}(\alpha, n)^{25}\text{Mg}$  cross section, as several inconsistencies on  $J^\pi$  were present in the literature prior to these measurements. In fact, five resonances were firmly identified below the lowest directly observed resonance in the  $^{22}\text{Ne}(\alpha, n)^{25}\text{Mg}$  cross section at  $E_\alpha \approx 830$  keV, as sketched in Figure 4.

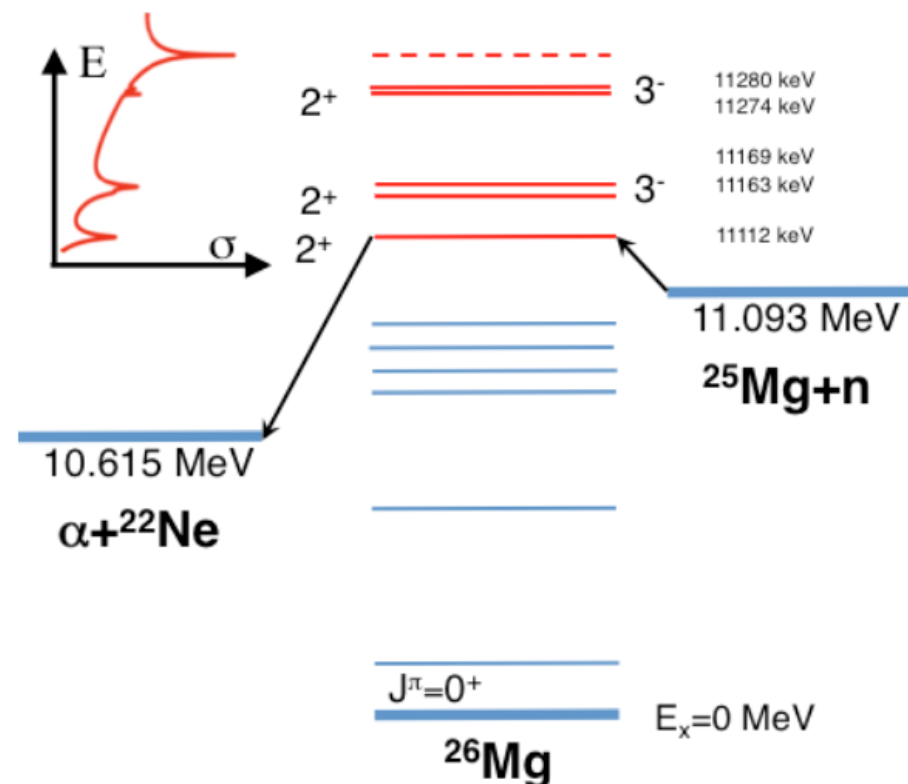


**Figure 4.** Level scheme of  $^{26}\text{Mg}$  with the  $^{25}\text{Mg}(n, \gamma)$  entrance channel and the  $^{22}\text{Ne}(\alpha, n)$  exit channel. The  $^{26}\text{Mg}$  levels characterised in terms of excitation energy and  $J^\pi$  by the collaborative effort of n\_TOF and GELINA are reported in red.

#### 4. Seed Isotopes

Several neutron capture reactions on s-process seeds have been measured at n\_TOF. The neutron capture yields and resonance parameters of the  $^{54}\text{Fe}(n, \gamma)$  and  $^{57}\text{Fe}(n, \gamma)$  reactions [45] have recently been provided to the IAEA EXFOR database<sup>3</sup>, to improve future evaluations of these cross sections. In addition, radiative neutron capture cross sections have been

studied for the case of  $^{58}\text{Ni}$  [46] and  $^{62}\text{Ni}$  [47,48]. For  $^{58}\text{Ni}(n, \gamma)$ , MACSs were determined from  $kT = 5\text{--}100$  keV with uncertainties lower than 6%. The MACS at  $kT = 30$  keV is in good agreement with previous data by Guber et al. [49], but 12% smaller than the recommended value of the KADoNiS 0.3 database [36]. The  $^{62}\text{Ni}(n, \gamma)$  MACS obtained at n\_TOF had the smallest uncertainty (4.5%) to date and was in good agreement at around  $kT = 30$  keV with most previous measurements [50–53].

After neutron capture on  $^{58}\text{Ni}$ , the long-lived radioisotope  $^{59}\text{Ni}$  (half-life  $7.6 \times 10^4$  years) is produced. At stellar neutron energies, the  $(n, \alpha)$  channel competes with  $(n, \gamma)$ , which leads to cycling material back to  $^{56}\text{Fe}$  in a star. This strengthens the role of  $^{56}\text{Fe}$  as an *s*-process seed. A measurement of the  $^{59}\text{Ni}(n, \alpha)$  reaction has been performed at n\_TOF using a new detection system based on sCVD diamond diodes. The first results were published in [54].

### 5. Magic Nuclei and End-Point

The relevance of neutron magic nuclei became apparent already when the first theory of *s*-process nucleosynthesis was postulated 60 years ago [1], owing to the prominent maxima in the solar system mass distribution at  $N = 50, 82$  and  $126$  (see Figure 1). Nuclei with a neutron-shell closure have a particularly stable nuclear structure, which translates into a relatively small neutron capture cross section, when compared to their non-magic neighbouring nuclei (see also Figure 5). As already mentioned in the introduction, this nuclear structure feature translates into a bottleneck effect in the flow of *s*-process matter in the nucleosynthesis of heavy isotopes.

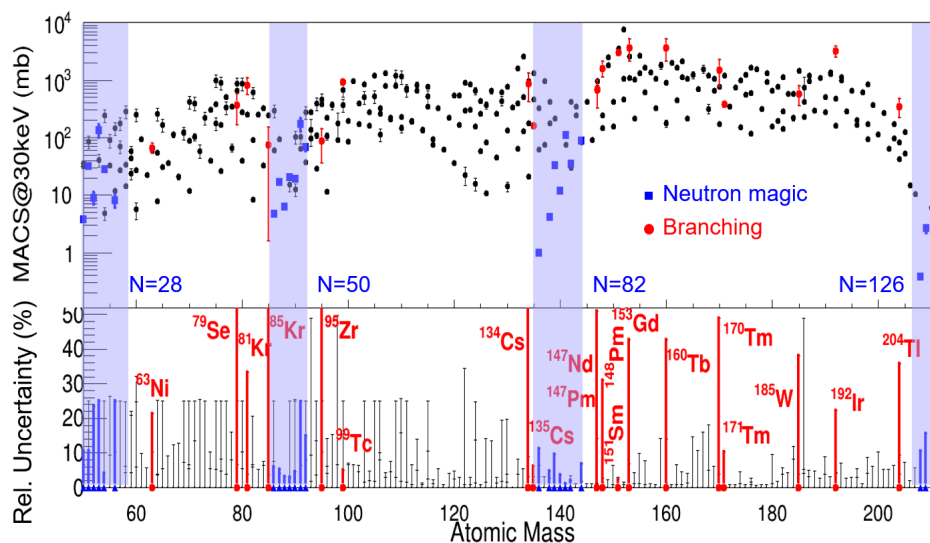


**Figure 5.** Maxwellian-averaged neutron capture cross section at 30 keV (top panel) and their relative uncertainties (bottom panel). Most values are taken from [42] (see text for details).

For small cross sections, the contribution from direct neutron capture (DRC) [55] may become important. As this component is nonresonant, it may be difficult to determine it with the time-of-flight technique, as it is hard to disentangle from the background. In these cases, measured MACSs need to be complemented by model calculations to account for DRC (this is the case, e.g., for Mg isotopes Mg [43] and  $^{58}\text{Ni}$  [46]).

From the experimental viewpoint, in most cases, the measurement of magic nuclei represents also a challenge owing to the very small radiative capture cross sections involved, which in some nuclei barely reach a few mb at  $kT = 30$  keV. This situation also implies that the radiative capture channel is much weaker than the competing elastic scattering channel. Typical elastic-to-capture ratios for these nuclei span between three and four orders of magnitude across the stellar energy range of interest. In these cases, the large number of scattered neutrons can interact promptly, or after some thermalisation, with the materials of

the experimental setup, thereby emitting radiation which contaminates the measurement and enhances the level of background. This effect, which is known as neutron sensitivity, has led to the development of optimised detection systems, such as the use of  $C_6D_6$  instead of the  $C_6F_6$  commonly employed in the early times [56].

At n\_TOF, carbon-fibre-based  $C_6D_6$  scintillation detectors were developed [26] aiming at the lowest possible neutron sensitivity. These developments turned out to be key to perform neutron capture measurements on neutron magic nuclei with a high accuracy. Thus, the first C-fibre versions of  $C_6D_6$  detectors were specifically applied at CERN's n\_TOF to measure the cross section of  $^{204,206,207}Pb$  [57–59] and  $^{209}Bi$  [60]. For several broad s-wave resonances with  $\Gamma_n/\Gamma_\gamma$  ratios of  $1 \times 10^3$  or larger, important deviations were found with respect to previously reported data. This effect can be most probably ascribed to a neutron-sensitivity bias in previous experiments, which is difficult to correct for. The measurement of the Pb and Bi isotopes contributed mainly to two different astrophysical aspects, which are discussed in the following. First, at the time of these experiments, *r*-process abundances were mostly based on the subtraction of the *s*-process contribution from the total solar-system abundances. These measurements thus provided important constraints to evaluate the performance of different mass models included in *r*-process model calculations used for reproducing the solar system abundances. This statement is illustrated in Figure 6, which shows the *r*-process residuals, obtained after subtracting the accurate *s*-process contributions from the total solar system abundances.

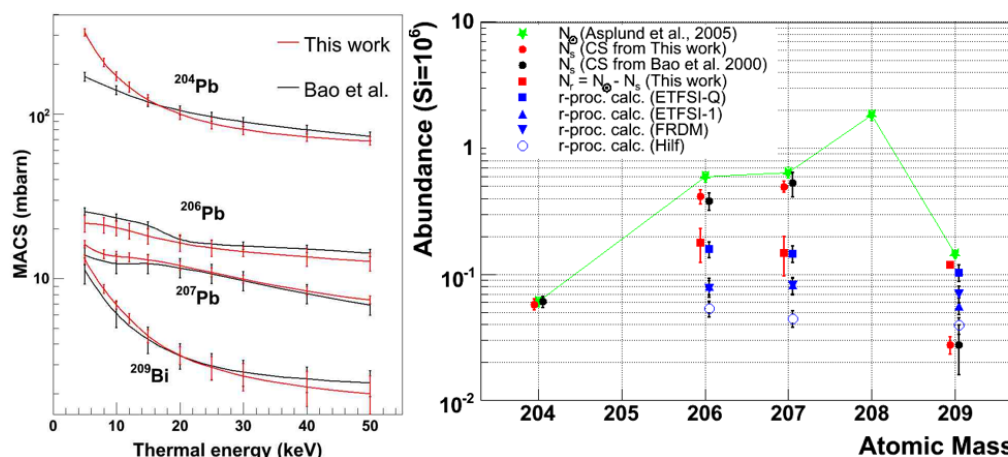


**Figure 6.** Maxwellian-averaged neutron capture cross sections for the  $^{204,206,207}Pb$  and  $^{209}Bi$  isotopes measured at CERN's n\_TOF (left panel). Solar system abundance analysis, with a disentanglement of the *r*-process component from the accurate *s*-process abundances (right panel). Furthermore, a comparison versus different *r*-process model calculations is shown, ruling out several of them.

Thus, instrument developments in terms of neutron sensitivity [26], in combination with improvements in the pulse height weighting technique [61], allowed us to obtain cross sections for the Pb and Bi isotopes with enhanced accuracy (see Figure 6). These results, in conjunction with stellar models [62], delivered rather accurate *s*-process contributions, which, particularly in the case of  $^{209}Bi$ , represented one of the most stringent constraints to *r*-process model calculations and their nuclear physics inputs (see Figure 6). In second place, these measurements helped to confirm the site of the main *s* process as low-mass ( $1.5M_\odot$ ,  $3M_\odot$ ) thermally pulsing AGB stars and in particular, the so-called strong *s*-process contribution, as the one arising from low-mass and low-metallicity ( $[Fe/H] = -0.3$ ,  $[Fe/H] = -1$ ) TP-AGB stars.

A further recent example is the measurement of the  $^{140}Ce(n,\gamma)$  cross section, which is one of the lowest along the *s*-process path. Preliminary results show sizeable differences with respect to the data in the literature [63]. Additional technical developments in instrumentation for neutron capture measurements of very low radiative neutron capture cross sections are discussed in Section 9.

## 6. S-Only Nuclei

To date, at n\_TOF, we have studied 4 of the 33 *s*-only isotopes along the *s*-process path:  $^{58}\text{Ni}$  [46],  $^{70}\text{Ge}$  [64],  $^{154}\text{Gd}$  [65] and  $^{186}\text{Os}$  [66,67]. Moreover, we plan to measure  $^{94,96}\text{Mo}(n,\gamma)$  in the near future. It is well known that the  $(n,\gamma)$  cross section for *s*-only isotopes has to be measured with high accuracy and precision, eventually resulting in small uncertainties [68]. Experimentally, measurements of radiative capture cross sections on *s*-only isotopes do not present particular challenges. However, when the isotope of interest features a small natural abundance, reaching the target uncertainty becomes exceedingly difficult. Instead of natural samples, enriched ones are required to perform accurate measurements. However, if the desired high level of enrichment cannot be produced or found, a viable option is to measure and analyse simultaneously the capture cross section of several (in principle all) stable isotopes of a given element, possibly using enriched samples.

This is the case of  $^{154}\text{Gd}(n,\gamma)$  cross Section [65] recently measured at n\_TOF together with  $^{155}\text{Gd}(n,\gamma)$  and  $^{157}\text{Gd}(n,\gamma)$  [69]. The enrichment of the available sample was only 66.78% in  $^{154}\text{Gd}$ , and the main contaminant was  $^{155}\text{Gd}$  and  $^{157}\text{Gd}$  to a minor extent. In order to cross-check the sample composition and minimise the related uncertainties, the capture data collected at n\_TOF were complemented by transmission measurements performed at GELINA. Overall, thanks to the combined  $^{154}\text{Gd}(n,\gamma)$  and  $^{155}\text{Gd}(n,\gamma)$  measurements and the availability of transmission data on the same sample from GELINA, the capture yield was determined accurately up to 300 keV. As a result, the MACS was reported from  $kT = 5\text{--}100$  keV with uncertainties lower than 6%, thus resolving a long-standing debate on the value of the cross section. In fact, prior to this measurement, the available MACS for  $kT = 30$  keV exhibited large differences ranging from 878(27) mb to 1278(102) mb. By confirming the previously reported data by Beer and collaborators [70], the n\_TOF MACS being 850(50) mb, we partially resolved a problem of underproduction of  $^{154}\text{Gd}$  nucleus in model calculations [18,71].

## 7. Branching Points of the *s* Process

Branching nuclei are unstable isotopes encountered along the *s*-process path, where a competition between neutron capture and  $\beta$ -decay takes place. For the neutron densities reached during core He-burning and shell C-burning in massive stars, and also in thermally pulsing AGB stars, the decay and capture timescales span from a few weeks up to several years. *S*-process branching nuclei are of paramount importance in nucleosynthesis studies, as they offer a unique opportunity to gain insight onto the physical conditions of the stellar environment such as temperature, neutron density or evolutionary timescales. For a recent systematic study, the reader is referred to [19] and references therein.

From the experimental point of view, branching nuclei represent one of the most challenging paradigms in the field of neutron capture cross section measurements. First, with very few exceptions, it is normally very difficult to produce a sufficiently large sample size for a cross-section measurement. For TOF measurements, sample masses of only a few milligrams have been measured [29], whereas the highly sensitive activation method has enabled the measurement of samples containing only 28 ng of material [72]. A further disadvantage is that, depending on the production mechanism, the sample may also contain a large portion of other contaminant isotopes. These impurities may represent an additional difficulty both for activation and TOF experiments. In TOF experiments, a high resolution becomes mandatory to separate the resonances from the different sample constituents. In activation measurements, a good spectroscopic resolution, such as that obtained with HPGe detectors, becomes necessary in order to disentangle transition levels between the isotope of interest and those from decays of other sample impurities. Finally, in TOF experiments the decay activity of the sample itself represents a conspicuous source of background. In fact,  $(n,\gamma)$  reaction cross section measurements on radioactive isotopes are challenging because the emitted  $\gamma$  rays originating from the decay cannot be easily disentangled from the prompt  $\gamma$ -ray cascade following the neutron capture reaction. This background can be a limitation in activation measurements, whereas for TOF measurements it can be

only minimised by means of a very high neutron luminosity. Sample activities of several hundreds of gigabecquerels have been successfully measured at n\_TOF [27–29]. However, for a given decay activity the feasibility of the measurement can vary a lot depending on the decay characteristics of the unstable nucleus.

The experimental situation for the major branching nuclei is illustrated in Figure 5, which shows that the uncertainties existing for the *s*-process branching isotopes (red) are still significantly large in most cases and typically much larger than those found for the stable neutron-magic isotopes (blue). This is to be ascribed to the aforesaid experimental challenges in sample production and limitations in state-of-the-art detection techniques and neutron-beam facilities.

Interestingly, only three *s*-process branching nuclei,  $^{99}\text{Tc}$  [73],  $^{135}\text{Cs}$  [74,75] and  $^{151}\text{Sm}$  [27], have been measured with an uncertainty of a few percent. This level of uncertainty is comparable to the corresponding uncertainty in the isotopic analysis of meteorites and, therefore, these measurements can be considered to have enough accuracy for a full assessment of their astrophysical implications. The neutron capture cross section measurement of  $^{99}\text{Tc}$  was one of the first *s*-process branching nuclei measured via TOF and it was used to constrain the time duration of the third dredge-up in low-mass AGB stars [73].

From about 23 main *s*-process branching isotopes, only five have been measured by means of the activation technique:  $^{135}\text{Cs}$  [74,75],  $^{147}\text{Pm}$  [72],  $^{155}\text{Eu}$  [76],  $^{163}\text{Ho}$  [77] and  $^{171}\text{Tm}$  [29]. However, in cases where the daughter nucleus is stable, only the time-of-flight method can be applied. Thus far, the TOF method has been utilised for the measurement of another five branching nuclei:  $^{63}\text{Ni}$  [28],  $^{99}\text{Tc}$  [73],  $^{151}\text{Sm}$  [27],  $^{171}\text{Tm}$  [29] and  $^{204}\text{Tl}$  [30], and there are plans to also measure  $^{79}\text{Se}$  in the near future at CERN's n\_TOF [78]. At present, in several cases, such as  $^{79}\text{Se}$ ,  $^{81,85}\text{Kr}$ ,  $^{95}\text{Zr}$ ,  $^{185}\text{W}$  and  $^{192}\text{Ir}$ , only theoretical calculations become available (see references cited in [42]), with typical discrepancies of a factor of two or more in the predicted MACS values. The cross section ascribed to these cases in Figure 5 corresponds to the average of the theoretical predictions available for each nucleus [42], while the uncertainty reflects the maximum deviation with respect to the average value. An aspect of pivotal importance for the measurement of the branching nuclei is the availability of suitable samples. In all cases, a sample needs to be specifically produced for the measurement, with ideally highest possible enrichment. Some *s*-process branching nuclei are particularly well suited to constrain the thermal conditions in TP-AGB stars. One such case is  $^{151}\text{Sm}$ , whose terrestrial half-life of  $t_{1/2} = 93$  y decreases to only a few years under stellar temperatures. The neutron capture cross section of this isotope was successfully measured at CERN's n\_TOF with a sample of 206 mg and an enrichment of 90% [27]. The result obtained for the MACS at 30 keV, 3100(160) mb, was above any previous theoretical prediction made until that time. The latter situation reflects the necessity of experimental nuclear data for a reliable assessment of astrophysical conditions. A significantly more challenging case was the recent measurement of  $^{171}\text{Tm}$  [29], with a half-life of only 1.92 y. In this case a sample of only 3 mg with an enrichment of 98% was available for a combined TOF and activation experiment at CERN's n\_TOF and SARAF-LiLiT, respectively. The MACS obtained was used to constrain the  $^{171}\text{Yb}$  abundance in the material lost by asymptotic giant branch stars, thereby providing an improved match to the available presolar SiC grain measurements.

## 8. Neutron Poisons and Neutron Captures on Light Elements

As mentioned in the introduction,  $^{14}\text{N}(n,p)$  and  $^{26}\text{Al}(n,p)$  reactions are considered the most important neutron poison reactions in AGB stars. Both of these reactions were recently measured at n\_TOF [79,80]. The high-flux beamline EAR-2 was chosen in both cases due to the low cross sections involved for  $^{14}\text{N}(n,p)$ , and the fact that a radioactive  $^{26}\text{Al}$  is only available in small quantities.

The  $^{26}\text{Al}(n,p)$  reaction was measured using a dedicated silicon strip detection system using a  $^{26}\text{Al}$  target of uniquely high areal density [81]. The new measurement provided resonance strengths for eleven resonances, nine being measured for the first time. The

resonance strengths are systematically lower than the only previous values available by Koehler et al. [82], and have a lower uncertainty. Cross sections were measured up to 150 keV neutron energy allowing to calculate the astrophysical reaction rates for stellar temperatures up to 0.5 GK, covering the range of interest to AGB stars. These rates were found to be higher compared to an activation measurement by Trautvetter et al. [83], however they are compatible within two sigmas.

The  $^{14}\text{N}(n,p)$  reaction has been studied with a silicon strip detection system, and an MMGAS detection system. The data analysis is currently ongoing.

In addition, and as mentioned above, we have measured the  $^{24,25,26}\text{Mg}(n,\gamma)$  cross sections [43]. Albeit marginal, the  $^{25}\text{Mg}(n,\gamma)$  reaction plays a non-negligible role when the  $^{22}\text{Ne}(\alpha,n)^{25}\text{Mg}$  source is activated. In fact, the large abundance of  $^{25}\text{Mg}$  makes it a significant neutron poison for the *s* process.

## 9. Future Perspectives

In the last decades a significant number of relevant measurements for *s*-process nucleosynthesis studies have been carried out, which were enabled after improvements in instrumentation [24–26,61,84], sample production techniques [85] and neutron-beam facilities [21,86]. Several examples have been discussed in the preceding sections, including measurements of milligram samples of unstable isotopes, with half-lives of only a few years and activities of hundreds of gigabecquerels. However, in many cases the final uncertainties on the cross sections are still sizeable, as it can be appreciated in Figure 5. This is certainly the case for several magic nuclei, and the situation is even more severe for many branching nuclei, where the error bars in most cases represent more than 20–30% of the measured cross-section value. In the cases where only theoretical calculations are available, like  $^{79}\text{Se}$ ,  $^{81,85}\text{Kr}$ ,  $^{95}\text{Zr}$ ,  $^{185}\text{W}$  or  $^{192}\text{Ir}$ , uncertainties are much higher (see Figure 5). For most cross sections of unstable nuclei the uncertainty level is significantly larger than the corresponding uncertainty on the *s*-process isotopic composition of meteorites and, therefore, the nuclear-physics input actually limits the astrophysics information that can be derived.

For many relevant branching nuclei, neutron capture leads to a stable isotope, where only the TOF method becomes applicable. In many cases [28–30], the main contribution to the cross-section uncertainty in the stellar energy range around 30 keV arises from the increasing contribution of neutron-induced backgrounds towards higher neutron energy. Owing to the decreasing signal-to-background ratio, it becomes increasingly difficult to observe resolved resonances beyond  $\sim 10$  keV. In this situation, either the URR needs to be analysed, with the correspondingly larger error bar, or a statistical analysis based on the levels measured at lower energy is carried out in order to extrapolate the cross section in the high neutron energy range, up to 100 keV [29]. In several important cases, neutrons scattered in the sample under study, and subsequently captured in the surroundings of the experimental setup, represent an important source of background and a limiting factor to obtain reliable data in the  $>10$  keV neutron energy range. One such example is the measurement of the  $^{93}\text{Zr}$  neutron capture cross section [87]. Using the cross section measured with the TOF technique [87], Neyskens et al. [88] determined an upper limit of  $2.5 \times 10^8$  K for the *s*-process temperature in low-mass asymptotic giant branch (AGB) stars. This result was obtained by comparing observations made with the HERMES spectrograph of the Zr=Nb abundance ratio in red giants and the experimental MACS values of the unstable  $^{93}\text{Zr}$  [87]. However, the temperature in AGB stars could be constrained further provided that the uncertainty of the measured cross section for  $^{93}\text{Zr}$ , 11%, would be smaller. To improve this situation and obtain more complete and accurate data in the kiloelectronvolt energy range of astrophysical interest, novel detection techniques are being developed. Some of these developments are discussed in the following.

With the aim of improving the signal-to-background ratio and enhance detection sensitivity in neutron capture TOF experiments the i-TED detection system is being developed in the framework of the ERC-funded project HYMNS [89]. i-TED stands for total energy

detector with  $\gamma$ -ray imaging capability [90]. This detector has been commissioned in 2021 and it will already become operational for neutron capture experiments in 2022 [78]. i-TED consists of an array of four Compton imagers with a large solid angle (Figure 7), which enable a further level of background rejection by exploiting  $\gamma$ -ray imaging techniques. Thus, it becomes possible on an event-by-event basis to obtain information on the spatial origin of each detected  $\gamma$  ray. When the registered  $\gamma$ -ray direction coincides with the position of the capture sample under study, the event can be accepted as a potentially true capture event. Otherwise, the event can be tagged as a background event most probably arising from contaminant neutron capture reactions in the surroundings of the experimental setup. An added advantage of i-TED is the high spectroscopic resolution of the embedded  $\text{LaCl}_3(\text{Ce})$  scintillation crystals, which also enables a deeper insight into the nuclear structure aspects of the reaction under study. i-TED will be applied for the first time in the measurement of  $^{79}\text{Se}(n, \gamma)$ , which is scheduled for 2022 at CERN's n\_TOF, utilizing both EAR1 and EAR2 [78].

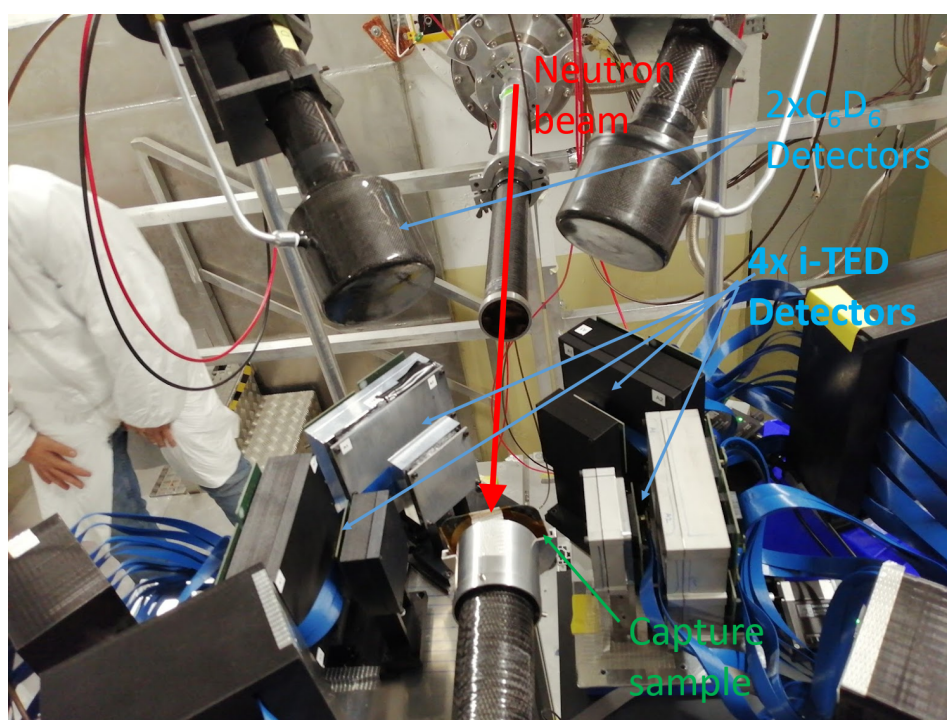


**Figure 7.** Photograph of the experimental setup at CERN's n\_TOF EAR1, for detector commissioning measurements in 2021. The sample is surrounded by two state-of-the-art C-fibre  $\text{C}_6\text{D}_6$  detectors and four i-TED Compton modules developed in the HYMNS ERC project [89].

In some other cases, a limiting factor in measuring a cross section up to high neutron energies ( $\sim 100$  keV) is the counting rate capability of the detector, which is related to its time response and its ability to measure many events in a short period of time. This is particularly important for the 20 m measuring station EAR2 at CERN's n\_TOF, where a very high neutron luminosity of  $10^6$  n/( $\text{cm}^2$  10 ms) becomes available. This performance is, on one hand, unique for the measurement of radioactive isotopes but, on the other hand, it cannot be fully exploited yet, due to limitations in detection systems, which struggle to cope with the large counting rates at very short TOF intervals. The segmented total energy detector (s-TED) is under development to cope with this experimental challenge. s-TED consists of an array of relatively small  $\text{C}_6\text{D}_6$ -detectors, which can handle in a more convenient way high gamma ray fluxes. At the moment, an array of nine s-TED detectors have been assembled at CIEMAT and some of them have been tested at CERN's n\_TOF with promising results during the commissioning runs of 2021. The aim is also to use silicon photomultipliers (SiPMs) instead of conventional photomultiplier tubes (PMTs),

which shall enable a lower intrinsic neutron sensitivity and better overall performance. Some prototypes based on SiPM readout have already been developed [91].

In order to complement and supplement the TOF measurements of astrophysical interest, the new NEAR station is being constructed and characterised at CERN's n\_TOF. NEAR will exploit the large neutron fluence attainable in the vicinity of the newly upgraded spallation target in order to perform highly sensitive activation measurements. A dedicated moderator-filter assembly based on a combination of borated polyethylene and aluminium will allow one to thermalise and shape the initially hard neutron spectrum and deliver a quasi-Maxwellian neutron distribution. The expected stellar energy ranges span from a few kiloelectronvolts up to almost 1 MeV, thereby covering the full stellar energy range of interest for the study of nucleosynthesis in TP-AGB stars. Figure 8 shows an example of the neutron distribution that can be obtained at thermal energies of around  $kT = 12$  keV, which is close to the thermal neutron energies of the shell H-burning stage in AGB stars in the interpulse periods.

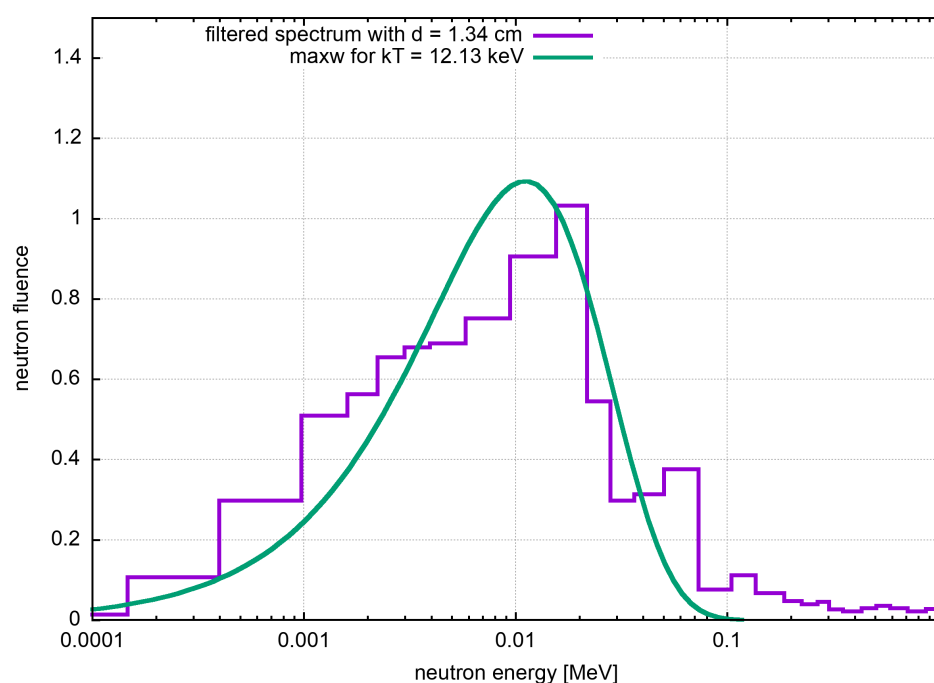


**Figure 8.** Preliminary results of simulations for the neutron energy distribution attainable at the NEAR station using a 30 cm thick aluminium fluoride moderator and a thin (1.34 cm) boron filter [92]. See text for details.

The attainable quasi-Maxwellian distributions, in general, will deviate significantly from the ideal case, an effect which can be corrected by means of accurate neutron energy distribution measurements and Monte Carlo simulations. At NEAR, in addition to the very broad neutron energy range covered, it will become possible to reach high neutron fluences, of the order of  $10^8$  to  $10^{10}$  n/cm<sup>2</sup>/pulse, depending on the final moderator/filter assembly chosen. However, rather than the attainable neutron intensity, the most singular aspect of the new facility will be its synergy with the neighbouring ISOLDE facility. In the latter it will be possible to synthesise isotopically pure samples of radioactive nuclei in very small quantities. This shall enable the first direct activation measurements at NEAR on unstable isotopes of astrophysical interest, never accessed thus far. A pneumatic rabbit system is under planning in order to transport the short-lived radioactive samples from ISOLDE to the NEAR station. A dedicated high-resolution  $\gamma$ -ray HPGe spectrometer has been already set up in order to measure the  $\gamma$ -rays from the decay of activated samples. At this moment several neutron flux characterization measurements are being performed at NEAR and it is expected that it will become operational in 1–2 years.

In summary, many different developments are taking place, which should enable in the next years exciting measurements and a deeper insight in many aspects of *s*-process nucleosynthesis in asymptotic giant branch stars.

## 10. Conclusions

The quest for accurate and new nuclear data on stable and radioactive isotopes for the study of the *s*-process nucleosynthesis has been partially addressed by the n\_TOF initiatives carried out so far and described in this article.

Some 37 isotopes, of which 7 are radioactive, have been studied and the results reported both in publications and in the publicly available experimental nuclear reaction database EXFOR. The measured cross sections are currently used in stellar model calculations to constraint and refine AGB stellar models. Other cross sections are being investigated, and analysis are ongoing. The related results are expected to be available soon.

In the next future, the n\_TOF collaboration plans to perform challenging cross-section measurements exploiting the improved characteristics of the renovated experimental areas EAR1 and EAR2, using the time-of-flight method. Furthermore, the brand-new irradiation station NEAR will enable activation measurements on short-lived isotopes.

In summary, the relevant n\_TOF scientific program related to the *s* process and AGB in particular, is foreseen to continuously improve in the next 10 years, at least.

**Author Contributions:** Writing—original draft, C.M., S.C., C.D.-P. and C.L.-W. Authors have equally contributed to the article. All authors have read and agreed to the published version of the manuscript.

**Funding:** CDP acknowledges funding from the European Research Council for the project HYMNS under ERC Consolidator Grant Agreement No. 681740 and from Spanish MICIN PID2019-104714GB-C21. CLW acknowledges support from the UK Science and Technologies Facilities Council (STFC), projects ST/P004008/1 and ST/M006085/1, and the European Research Council ERC-2015-STG No. 677497.

**Data Availability Statement:** The cross section data referred in this article are available on EXFOR and the references cited.

**Acknowledgments:** We would like to acknowledge Franz Käppeler, who sadly passed away recently. His contribution to the n\_TOF research activities and the field of nuclear astrophysics in general was profound and many of the results and research successes described here are owed to his great enthusiasm and support.

**Conflicts of Interest:** The authors declare no conflict of interest.

## Notes

<sup>1</sup> In terms of the center-of-mass energy  $E$  it can be expressed as:

$$\phi_{MB}(v)dv = \phi_{MB}(E)dE = \frac{2}{\sqrt{\pi}} \frac{1}{(kT)^{3/2}} \sqrt{E} e^{-\frac{E}{kT}} dE$$

or alternatively, in terms of relative velocity:

$$\phi_{MB}(v)dv = 4\pi v^2 \left( \frac{\mu}{2\pi kT} \right)^{3/2} e^{-\frac{\mu v^2}{2kT}} dv.$$

<sup>2</sup> The contribution from the so-called *p* process (i.e., proton capture and photodisintegration reactions) to these abundances is typically two orders of magnitude smaller.

<sup>3</sup> <https://www.nds.iaea.org/exfor/> (accessed on 8 December 2021).

## References

1. Burbidge, E.M.; Burbidge, G.R.; Fowler, W.A.; Hoyle, F. Synthesis of the Elements in Stars. *Rev. Mod. Phys.* **1957**, *29*, 547–650. [[CrossRef](#)]
2. Busso, M.; Gallino, R.; Wasserburg, G.J. Nucleosynthesis in Asymptotic Giant Branch Stars: Relevance for Galactic Enrichment and Solar System Formation. *Annu. Rev. Astron. Astrophys.* **1999**, *37*, 239–309. [[CrossRef](#)]
3. Herwig, F. Evolution of Asymptotic Giant Branch Stars. *Annu. Rev. Astron. Astrophys.* **2005**, *43*, 435–479. [[CrossRef](#)]
4. Straniero, O.; Gallino, R.; Cristallo, S. s process in low-mass asymptotic giant branch stars. *Nucl. Phys. A* **2006**, *777*, 311–339. [[CrossRef](#)]
5. Karakas, A.I.; Lattanzio, J.C. The Dawes Review 2: Nucleosynthesis and Stellar Yields of Low- and Intermediate-Mass Single Stars. *Publ. Astron. Soc. Aust.* **2014**, *31*, e030. [[CrossRef](#)]
6. Pignatari, M.; Gallino, R.; Heil, M.; Wiescher, M.; Käppeler, F.; Herwig, F.; Bisterzo, S. The Weak s-Process in Massive Stars and its Dependence on the Neutron Capture Cross Sections. *Astrophys. J.* **2010**, *710*, 1557–1577. [[CrossRef](#)]
7. Wallner, A.; Buczak, K.; Dillmann, I.; Feige, J.; Käppeler, F.; Korschinek, G.; Lederer, C.; Mengoni, A.; Ott, U.; Paul, M.; et al. AMS Applications in Nuclear Astrophysics: New Results for  $^{13}\text{C}(n,\gamma)^{14}\text{C}$  and  $^{14}\text{N}(n,p)^{14}\text{C}$ . *Publ. Astron. Soc. Aust.* **2012**, *29*, 115–120. [[CrossRef](#)]
8. Straniero, O.; Gallino, R.; Busso, M.; Chieffi, A.; Raiteri, C.M.; Limongi, M.; Salaris, M. Radiative  $^{13}\text{C}$  Burning in Asymptotic Giant Branch Stars and s-Processing. *Astrophys. J. Lett.* **1995**, *440*, L85. [[CrossRef](#)]
9. Cristallo, S.; La Cognata, M.; Massimi, C.; Best, A.; Palmerini, S.; Straniero, O.; Trippella, O.; Busso, M.; Ciani, G.F.; Mingrone, F.; et al. The Importance of the  $^{13}\text{C}(\alpha,n)^{16}\text{O}$  Reaction in Asymptotic Giant Branch Stars. *Astrophys. J.* **2018**, *859*, 105. [[CrossRef](#)]
10. Vescovi, D.; Cristallo, S.; Busso, M.; Liu, N. Magnetic-buoyancy-induced Mixing in AGB Stars: Presolar SiC Grains. *Astrophys. J. Lett.* **2020**, *897*, L25. [[CrossRef](#)]
11. Busso, M.; Vescovi, D.; Palmerini, S.; Cristallo, S.; Antonuccio-Delogu, V. s-processing in AGB Stars Revisited. III. Neutron Captures from MHD Mixing at Different Metallicities and Observational Constraints. *Astrophys. J.* **2021**, *908*, 55. [[CrossRef](#)]
12. Palmerini, S.; Busso, M.; Vescovi, D.; Naselli, E.; Pidotella, A.; Mucciola, R.; Cristallo, S.; Mascali, D.; Mengoni, A.; Simonucci, S.; et al. Presolar Grain Isotopic Ratios as Constraints to Nuclear and Stellar Parameters of Asymptotic Giant Branch Star Nucleosynthesis. *Astrophys. J.* **2021**, *921*, 7. [[CrossRef](#)]
13. Battino, U.; Pignatari, M.; Ritter, C.; Herwig, F.; Denisenkov, P.; Den Hartogh, J.W.; Trappitsch, R.; Hirschi, R.; Freytag, B.; Thielemann, F.; et al. Application of a Theory and Simulation-based Convective Boundary Mixing Model for AGB Star Evolution and Nucleosynthesis. *Astrophys. J.* **2016**, *827*, 30. [[CrossRef](#)]
14. Ciani, G.F.; Csedreki, L.; Rapagnani, D.; Aliotta, M.; Balibrea-Correa, J.; Barile, F.; Bemmerer, D.; Best, A.; Boeltzig, A.; Broggini, C.; et al. Direct Measurement of the C 13 ( $\alpha,n$ )O 16 Cross Section into the s-Process Gamow Peak. *Phys. Rev. Lett.* **2021**, *127*, 152701. [[CrossRef](#)] [[PubMed](#)]
15. Adsley, P.; Battino, U.; Best, A.; Caciolli, A.; Guglielmetti, A.; Imbriani, G.; Jayatissa, H.; La Cognata, M.; Lamia, L.; Masha, E.; et al. Reevaluation of the  $^{22}\text{Ne}(\alpha,\gamma)^{26}\text{Mg}$  and  $^{22}\text{Ne}(\alpha,n)^{25}\text{Mg}$  reaction rates. *Phys. Rev. C* **2021**, *103*, 015805. [[CrossRef](#)]
16. Koloczek, A.; Thomas, B.; Glorius, J.; Plag, R.; Pignatari, M.; Reifarth, R.; Ritter, C.; Schmidt, S.; Sonnabend, K. Sensitivity study for s process nucleosynthesis in AGB stars. *At. Data Nucl. Data Tables* **2016**, *108*, 1–14. [[CrossRef](#)]
17. Cristallo, S.; Straniero, O.; Gallino, R.; Piersanti, L.; Domínguez, I.; Lederer, M.T. Evolution, Nucleosynthesis, and Yields of Low-Mass Asymptotic Giant Branch Stars at Different Metallicities. *Astrophys. J.* **2009**, *696*, 797–820. [[CrossRef](#)]
18. Prantzos, N.; Abia, C.; Cristallo, S.; Limongi, M.; Chieffi, A. Chemical evolution with rotating massive star yields II. A new assessment of the solar s- and r-process components. *Mon. Not. R. Astron. Soc.* **2020**, *491*, 1832–1850. [[CrossRef](#)]
19. Bisterzo, S.; Gallino, R.; Käppeler, F.; Wiescher, M.; Imbriani, G.; Straniero, O.; Cristallo, S.; Görres, J.; de Boer, R.J. The branchings of the main s-process: Their sensitivity to  $\alpha$ -induced reactions on  $^{13}\text{C}$  and  $^{22}\text{Ne}$  and to the uncertainties of the nuclear network. *Mon. Not. R. Astron. Soc.* **2015**, *449*, 506–527. [[CrossRef](#)]
20. Cristallo, S.; Straniero, O.; Piersanti, L.; Gobrecht, D. Evolution, Nucleosynthesis, and Yields of AGB Stars at Different Metallicities. III. Intermediate-mass Models, Revised Low-mass Models, and the ph-FRUIITY Interface. *Astrophys. J. Suppl. Ser.* **2015**, *219*, 40. [[CrossRef](#)]
21. Guerrero, C.; Tsinganis, A.; Berthoumieux, E.; Barbagallo, M.; Belloni, F.; Günsing, F.; Weiß, C.; Chiaveri, E.; Calviani, M.; Vlachoudis, V.; et al. Performance of the neutron time-of-flight facility n\_TOF at CERN. *Eur. Phys. J. A* **2013**, *49*, 27. [[CrossRef](#)]
22. Barbagallo, M.; Guerrero, C.; Tsinganis, A.; Tarrío, D.; Altstadt, S.; Andriamonje, S.; Andrzejewski, J.; Audouin, L.; Bécares, V.; Bečvář, F.; et al. High-accuracy determination of the neutron flux at n\_TOF. *Eur. Phys. J. A* **2013**, *49*, 156. [[CrossRef](#)]
23. Sabaté-Gilarte, M.; Barbagallo, M.; Colonna, N.; Günsing, F.; Žugec, P.; Vlachoudis, V.; Chen, Y.H.; Stamatopoulos, A.; Leredegui-Marco, J.; Cortés-Giraldo, M.A.; et al. High-accuracy determination of the neutron flux in the new experimental area n\_TOF-EAR2 at CERN. *Eur. Phys. J. A* **2017**, *53*, 210. [[CrossRef](#)]
24. Guerrero, C.; Cano-Ott, D.; Mendoza, E.; Tañá, J.L.; Algora, A.; Berthoumieux, E.; Colonna, N.; Domingo-Pardo, C.; González-Romero, E.; Heil, M.; et al. Monte Carlo simulation of the n\_TOF Total Absorption Calorimeter. *Nucl. Instrum. Methods Phys. Res. A* **2012**, *671*, 108–117. [[CrossRef](#)]
25. Guerrero, C.; Cano-Ott, D.; Mendoza, E.; Wright, T. Correction of dead-time and pile-up in a detector array for constant and rapidly varying counting rates. *Nucl. Instrum. Methods Phys. Res. A* **2015**, *777*, 63–69. [[CrossRef](#)]

26. Plag, R.; Heil, M.; Käppeler, F.; Pavlopoulos, P.; Reifarh, R.; Wisshak, K.; n TOF Collaboration. An optimized C<sub>6</sub>D<sub>6</sub> detector for studies of resonance-dominated (n,γ) cross-sections. *Nucl. Instrum. Methods Phys. Res. A* **2003**, *496*, 425–436. [[CrossRef](#)]
27. Abbondanno, U.; Aerts, G.; Alvarez-Velarde, F.; Álvarez-Pol, H.; Andriamonje, S.; Andrzejewski, J.; Badurek, G.; Baumann, P.; Bečvář, F.; Benlliure, J.; et al. Neutron Capture Cross Section Measurement of <sup>151</sup>Sm at the CERN Neutron Time of Flight Facility (n\_TOF). *Phys. Rev. Lett.* **2004**, *93*, 161103. [[CrossRef](#)] [[PubMed](#)]
28. Lederer, C.; Massimi, C.; Altstadt, S.; Andrzejewski, J.; Audouin, L.; Barbagallo, M.; Bécaries, V.; Bečvář, F.; Belloni, F.; Berthoumieux, E.; et al. Neutron Capture Cross Section of Unstable Ni63: Implications for Stellar Nucleosynthesis. *Phys. Rev. Lett.* **2013**, *110*, 022501. [[CrossRef](#)] [[PubMed](#)]
29. Guerrero, C.; Lerendegui-Marco, J.; Paul, M.; Tessler, M.; Heinitz, S.; Domingo-Pardo, C.; Cristallo, S.; Dressler, R.; Halfon, S.; Kivel, N.; et al. Neutron Capture on the s-Process Branching Point Tm 171 via Time-of-Flight and Activation. *Phys. Rev. Lett.* **2020**, *125*, 142701. [[CrossRef](#)]
30. Casanovas, A.; Tarifeño-Saldivia, A.E.; Domingo-Pardo, C.; Calviño, F.; Maugeri, E.; Guerrero, C.; Lerendegui-Marco, J.; Dressler, R.; Heinitz, S.; Schumann, D.; et al. Neutron capture measurement at the n TOF facility of the <sup>204</sup>Tl and <sup>205</sup>Tl s-process branching points. *J. Phys. Conf. Ser.* **2020**, *1668*, 012005. [[CrossRef](#)]
31. Esposito, R.; Calviani, M.; Aberle, O.; Barbagallo, M.; Cano-Ott, D.; Coiffet, T.; Colonna, N.; Domingo-Pardo, C.; Dragoni, F.; Franqueira Ximenes, R.; et al. Design of the third-generation lead-based neutron spallation target for the neutron time-of-flight facility at CERN. *Phys. Rev. Accel. Beams* **2021**, *24*, 093001. [[CrossRef](#)]
32. Mondelers, W.; Schillebeeckx, P. GELINA, a Neutron Time-of-Flight Facility for High-Resolution Neutron Data Measurements. Research Infrastructures II (2). 2006. Available online: <https://publications.jrc.ec.europa.eu/repository/handle/JRC35644> (accessed on 8 December 2021).
33. Paul, M.; Tessler, M.; Friedman, M.; Halfon, S.; Palchan, T.; Weissman, L.; Arenshtam, A.; Berkovits, D.; Eisen, Y.; Eliahu, I.; et al. Reactions along the astrophysical s-process path and prospects for neutron radiotherapy with the Liquid-Lithium Target (LiLiT) at the Soreq Applied Research Accelerator Facility (SARAF). *Eur. Phys. J. A* **2019**, *55*, 44. [[CrossRef](#)]
34. Ratynski, W.; Käppeler, F. Neutron capture cross section of <sup>197</sup>Au: A standard for stellar nucleosynthesis. *Phys. Rev. C* **1988**, *37*, 595–604. [[CrossRef](#)] [[PubMed](#)]
35. Macklin, R.L.; Halperin, J.; Winters, R.R. Gold neutron-capture cross section from 3 to 550 keV. *Phys. Rev. C* **1975**, *11*, 1270–1279. [[CrossRef](#)]
36. Dillmann, I.; Käppeler, F.; Plag, R.; Rauscher, T.; Thielemann, F. KADoNiS v0.3—The third update of the “Karlsruhe Astrophysical Database of Nucleosynthesis in Stars”. In *EFNUDAT Fast Neutrons, Proceedings of the Scientific Workshop on Neutron Measurements, Theory and Applications—Nuclear Data for Sustainable Nuclear Energy, Geel, Belgium 28–30 April 2009*; Hamsch, F., Ed.; EUR 23883 EN; Publications Office of the European Union: Luxembourg, 2010; JRC56548, p. 123; [[CrossRef](#)]
37. Massimi, C.; Domingo-Pardo, C.; Vannini, G.; Audouin, L.; Guerrero, C.; Abbondanno, U.; Aerts, G.; Álvarez, H.; Álvarez-Velarde, F.; Andriamonje, S.; et al. Au197(n,γ) cross section in the resonance region. *Phys. Rev. C* **2010**, *81*, 044616. [[CrossRef](#)]
38. Lederer, C.; Colonna, N.; Domingo-Pardo, C.; Günsing, F.; Käppeler, F.; Massimi, C.; Mengoni, A.; Wallner, A.; Abbondanno, U.; Aerts, G.; et al. Au197(n,γ) cross section in the unresolved resonance region. *Phys. Rev. C* **2011**, *83*, 034608. [[CrossRef](#)]
39. Massimi, C.; Becker, B.; Dupont, E.; Kopecky, S.; Lampoudis, C.; Massarczyk, R.; Moxon, M.; Pronyaev, V.; Schillebeeckx, P.; Sirakov, I.; et al. Neutron capture cross section measurements for <sup>197</sup>Au from 3.5 to 84 keV at GELINA. *Eur. Phys. J. A* **2014**, *50*, 124. [[CrossRef](#)]
40. Sirakov, I.; Becker, B.; Capote, R.; Dupont, E.; Kopecky, S.; Massimi, C.; Schillebeeckx, P. Results of total cross section measurements for <sup>197</sup>Au in the neutron energy region from 4 to 108 keV at GELINA. *Eur. Phys. J. A* **2013**, *49*, 144. [[CrossRef](#)]
41. Reifarh, R.; Erbacher, P.; Fiebiger, S.; Göbel, K.; Heftrich, T.; Heil, M.; Käppeler, F.; Klapper, N.; Kurtulgil, D.; Langer, C.; et al. Neutron-induced cross sections. From raw data to astrophysical rates. *Eur. Phys. J. Plus* **2018**, *133*, 424. [[CrossRef](#)]
42. Dillmann, I. The new KADoNiS v1.0 and its influence on the s-process. In *Proceedings of the Science, XIII Nuclei in the Cosmos (NIC XIII)*, Debrecen, Hungary, 7–11 July 2014; p. 57. [[CrossRef](#)]
43. Massimi, C.; Koehler, P.; Bisterzo, S.; Colonna, N.; Gallino, R.; Günsing, F.; Käppeler, F.; Lorusso, G.; Mengoni, A.; Pignatari, M.; et al. Resonance neutron-capture cross sections of stable magnesium isotopes and their astrophysical implications. *Phys. Rev. C* **2012**, *85*, 044615. [[CrossRef](#)]
44. Massimi, C.; Altstadt, S.; Andrzejewski, J.; Audouin, L.; Barbagallo, M.; Bécaries, V.; Bečvář, F.; Belloni, F.; Berthoumieux, E.; Billowes, J.; et al. Neutron spectroscopy of <sup>26</sup>Mg states: Constraining the stellar neutron source <sup>22</sup>Ne(α,n)<sup>25</sup>Mg. *Phys. Lett. B* **2017**, *768*, 1–6. [[CrossRef](#)]
45. Giubrone, G.; Domingo-Pardo, C.; Taín, J.L.; Lederer, C.; Altstadt, S.; Andrzejewski, J.; Audouin, L.; Barbagallo, M.; Bécaries, V.; Bečvář, F.; et al. Measurement of the <sup>54,57</sup>Fe(n,γ) Cross Section in the Resolved Resonance Region at CERN n\_TOF. *Nucl. Data Sheets* **2014**, *119*, 117–120. [[CrossRef](#)]
46. Žugec, P.; Barbagallo, M.; Colonna, N.; Bosnar, D.; Altstadt, S.; Andrzejewski, J.; Audouin, L.; Bécaries, V.; Bečvář, F.; Belloni, F.; et al. Experimental neutron capture data of <sup>58</sup>Ni from the CERN n\_TOF facility. *Phys. Rev. C* **2014**, *89*, 014605. [[CrossRef](#)]
47. Lederer, C.; Massimi, C.; Berthoumieux, E.; Colonna, N.; Dressler, R.; Guerrero, C.; Günsing, F.; Käppeler, F.; Kivel, N.; Pignatari, M.; et al. Ni62(n,γ) and Ni63(n,γ) cross sections measured at the n\_TOF facility at CERN. *Phys. Rev. C* **2014**, *89*, 025810. [[CrossRef](#)]

48. Lederer, C.; Massimi, C.; Berthoumieux, E.; Colonna, N.; Dressler, R.; Guerrero, C.; Günsing, F.; Käppeler, F.; Kivel, N.; Pignatari, M.; et al. Erratum:  $^{62}\text{Ni}(n,\gamma)$  and  $^{63}\text{Ni}(n,\gamma)$  cross sections measured at the n\_TOF facility at CERN [Phys. Rev. C 89, 025810 (2014)]. *Phys. Rev. C* **2015**, *92*, 019903. [[CrossRef](#)]
49. Guber, K.H.; Derrien, H.; Leal, L.C.; Arbanas, G.; Wiarda, D.; Koehler, P.E.; Harvey, J.A. Astrophysical reaction rates for  $\text{Ni}58,60(n,\gamma)$  from new neutron capture cross section measurements. *Phys. Rev. C* **2010**, *82*, 057601.
50. Alpizar-Vicente, A.M.; Bredeweg, T.A.; Esch, E.I.; Greife, U.; Haight, R.C.; Hatarik, R.; O'Donnell, J.M.; Reifarth, R.; Rundberg, R.S.; Ullmann, J.L.; et al. Neutron capture cross section of  $\text{Ni}62$  at s-process energies. *Phys. Rev. C* **2008**, *77*, 015806. [[CrossRef](#)]
51. Nassar, H.; Paul, M.; Ahmad, I.; Berkovits, D.; Bettan, M.; Collon, P.; Dababneh, S.; Ghelberg, S.; Greene, J.P.; Heger, A.; et al. Stellar  $(n,\gamma)$  Cross Section of  $^{62}\text{Ni}$ . *Phys. Rev. Lett.* **2005**, *94*, 092504. [[CrossRef](#)]
52. Walter, S. Wissenschaftliche Berichte, FZKA-7411 (August 2008) Dissertation, Universität Karlsruhe 2008, Universität Karlsruhe (TH). Ph.D Thesis, University of Karlsruhe, Karlsruhe, Germany, 2008.
53. Dillmann, I.; Faestermann, T.; Korschinek, G.; Lachner, J.; Maiti, M.; Poutivtsev, M.; Rugel, G.; Walter, S.; Käppeler, F.; Erhard, M.; et al. Solving the stellar  $^{62}\text{Ni}$  problem with AMS. *Nucl. Instrum. Methods Phys. Res. Sect. B Beam Interact. Mater. Atoms* **2010**, *268*, 1283–1286. [[CrossRef](#)]
54. Weiss, C.; Guerrero, C.; Griesmayer, E.; Andrzejewski, J.; Badurek, G.; Chiaveri, E.; Dressler, R.; Ganesan, S.; Jericha, E.; Kappeler, F.; et al. The  $(n,\hat{\alpha})$  Reaction in the s-process Branching Point  $^{59}\text{Ni}$ . *Nucl. Data Sheets* **2014**, *120*, 208–210. [[CrossRef](#)]
55. Mengoni, A.; Otsuka, T.; Ishihara, M. Direct radiative capture of p-wave neutrons. *Phys. Rev. C* **1995**, *52*, R2334–R2338. [[CrossRef](#)] [[PubMed](#)]
56. Corvi, F.; Prevignano, A.; Liskien, H.; Smith, P.B. An experimental method for determining the total efficiency and the response function of a gamma-ray detector in the range 0.5–10 MeV. *Nucl. Instrum. Methods Phys. Res. A* **1988**, *265*, 475–484. [[CrossRef](#)]
57. Domingo-Pardo, C.; Abbondanno, U.; Aerts, G.; Álvarez-Pol, H.; Alvarez-Velarde, F.; Andriamonje, S.; Andrzejewski, J.; Assimakopoulos, P.; Audouin, L.; Badurek, G.; et al. Measurement of the neutron capture cross section of the s-only isotope  $\text{Pb}204$  from 1 eV to 440 keV. *Phys. Rev. C* **2007**, *75*, 015806. [[CrossRef](#)]
58. Domingo-Pardo, C.; Abbondanno, U.; Aerts, G.; Álvarez, H.; Alvarez-Velarde, F.; Andriamonje, S.; Andrzejewski, J.; Assimakopoulos, P.; Audouin, L.; Badurek, G.; et al. Measurement of the radiative neutron capture cross section of  $\text{Pb}206$  and its astrophysical implications. *Phys. Rev. C* **2007**, *76*, 045805. [[CrossRef](#)]
59. Domingo-Pardo, C.; Abbondanno, U.; Aerts, G.; Álvarez-Pol, H.; Alvarez-Velarde, F.; Andriamonje, S.; Andrzejewski, J.; Assimakopoulos, P.; Audouin, L.; Badurek, G.; et al. Resonance capture cross section of  $\text{Pb}207$ . *Phys. Rev. C* **2006**, *74*, 055802. [[CrossRef](#)]
60. Domingo-Pardo, C.; Abbondanno, U.; Aerts, G.; Álvarez-Pol, H.; Alvarez-Velarde, F.; Andriamonje, S.; Andrzejewski, J.; Assimakopoulos, P.; Audouin, L.; Badurek, G.; et al. New measurement of neutron capture resonances in  $\text{Bi}209$ . *Phys. Rev. C* **2006**, *74*, 025807. [[CrossRef](#)]
61. Abbondanno, U.; Aerts, G.; Alvarez, H.; Andriamonje, S.; Angelopoulos, A.; Assimakopoulos, P.; Bacri, C.O.; Badurek, G.; Baumann, P.; Bečvář, F.; et al. New experimental validation of the pulse height weighting technique for capture cross-section measurements. *Nucl. Instrum. Methods Phys. Res. A* **2004**, *521*, 454–467. [[CrossRef](#)]
62. Gallino, R.; Arlandini, C.; Busso, M.; Lugaro, M.; Travaglio, C.; Straniero, O.; Chieffi, A.; Limongi, M. Evolution and Nucleosynthesis in Low-Mass Asymptotic Giant Branch Stars. II. Neutron Capture and the S-Process. *Astrophys. J.* **1998**, *497*, 388–403. [[CrossRef](#)]
63. Amaducci, S.; Colonna, N.; Cosentino, L.; Cristallo, S.; Finocchiaro, P.; Kr̨t̨icka, M.; Massimi, C.; Mastromarco, M.; Mazzone, A.; Mengoni, A.; et al. First Results of the  $^{140}\text{Ce}(n,\gamma)^{141}\text{Ce}$  Cross-Section Measurement at n\_TOF. *Universe* **2021**, *7*, 200. [[CrossRef](#)]
64. Gawlik, A.; Lederer-Woods, C.; Andrzejewski, J.; Battino, U.; Ferreira, P.; Günsing, F.; Heinitz, S.; Kr̨t̨icka, M.; Massimi, C.; Mingrone, F.; et al. Measurement of the  $^{70}\text{Ge}(n,\gamma)$  cross section up to 300 keV at the CERN n\_TOF facility. *Phys. Rev. C* **2019**, *100*, 045804. [[CrossRef](#)]
65. Mazzone, A.; Cristallo, S.; Aberle, O.; Alaerts, G.; Alcayne, V.; Amaducci, S.; Andrzejewski, J.; Audouin, L.; Babiano-Suarez, V.; Bacak, M.; et al. Measurement of the  $^{154}\text{Gd}(n,\gamma)$  cross section and its astrophysical implications. *Phys. Lett. B* **2020**, *804*, 135405. [[CrossRef](#)]
66. Mosconi, M.; Fujii, K.; Mengoni, A.; Domingo-Pardo, C.; Käppeler, F.; Abbondanno, U.; Aerts, G.; Álvarez-Pol, H.; Alvarez-Velarde, F.; Andriamonje, S.; et al. Neutron physics of the Re/Os clock. I. Measurement of the  $(n,\gamma)$  cross sections of  $\text{Os}186,187,188$  at the CERN n\_TOF facility. *Phys. Rev. C* **2010**, *82*, 015802. [[CrossRef](#)]
67. Fujii, K.; Mosconi, M.; Mengoni, A.; Domingo-Pardo, C.; Käppeler, F.; Abbondanno, U.; Aerts, G.; Álvarez-Pol, H.; Alvarez-Velarde, F.; Andriamonje, S.; et al. Neutron physics of the Re/Os clock. III. Resonance analyses and stellar  $(n,\gamma)$  cross sections of  $\text{Os}186,187,188$ . *Phys. Rev. C* **2010**, *82*, 015804. [[CrossRef](#)]
68. Käppeler, F. Stellar neutron capture rates—Key data for the s process. *Eur. Phys. J. Web Conf.* **2013**, *63*, 03002.
69. Mastromarco, M.; Manna, A.; Aberle, O.; Andrzejewski, J.; Audouin, L.; Bacak, M.; Balibrea, J.; Barbagallo, M.; Bečvář, F.; Berthoumieux, E.; et al. Cross section measurements of  $^{155,157}\text{Gd}(n,\gamma)$  induced by thermal and epithermal neutrons. *Eur. Phys. J. A* **2019**, *55*, 9. [[CrossRef](#)]
70. Beer, H.; Macklin, R.L. The  $^{151}\text{Sm}$  Branching: A Probe for the Irradiation Time Scale of the s-Process. *Astrophys. J.* **1988**, *331*, 1047.
71. Cristallo, S.; Abia, C.; Straniero, O.; Piersanti, L. On the Need for the Light Elements Primary Process (LEPP). *Astrophys. J.* **2015**, *801*, 53. [[CrossRef](#)]

72. Reifarh, R.; Arlandini, C.; Heil, M.; Käppeler, F.; Sedyshev, P.V.; Mengoni, A.; Herman, M.; Rauscher, T.; Gallino, R.; Travaglio, C. Stellar Neutron Capture on Promethium: Implications for the s-Process Neutron Density. *Astrophys. J.* **2003**, *582*, 1251–1262. [[CrossRef](#)]
73. Winters, R.R.; Macklin, R.L. Maxwellian-averaged Neutron Capture Cross Sections for  $^{99}\text{Tc}$  and  $^{95-98}\text{Mo}$ . *Astrophys. J.* **1987**, *313*, 808. [[CrossRef](#)]
74. Jaag, S.; Käppeler, F.; Koehler, P. The Stellar  $(n, \gamma)$  Cross Section of the Unstable  $^{135}\text{Cs}$ . *Nucl. Phys. A* **1997**, *621*, 247–250. [[CrossRef](#)]
75. Patronis, N.; Dababneh, S.; Assimakopoulos, P.A.; Gallino, R.; Heil, M.; Käppeler, F.; Karamanis, D.; Koehler, P.E.; Mengoni, A.; Plag, R. Neutron capture studies on unstable  $^{135}\text{Cs}$  for nucleosynthesis and transmutation. *Phys. Rev. C* **2004**, *69*, 025803.
76. Jaag, S.; Käppeler, F. Stellar  $(n, \gamma)$  cross section of the unstable isotope  $^{155}\text{Eu}$ . *Phys. Rev. C* **1995**, *51*, 3465–3471. [[CrossRef](#)] [[PubMed](#)]
77. Jaag, S.; Käppeler, F. The Stellar  $(n, \gamma)$  Cross Section of the Unstable Isotope  $^{163}\text{Ho}$  and the Origin of  $^{164}\text{Er}$ . *Astrophys. J.* **1996**, *464*, 874. [[CrossRef](#)]
78. Babiano-Suárez, V.; Balibrea-Correa, J.; Caballero, L.; Calviño, F.; Cano-Ott, D.; Casanovas, A.; Colonna, N.; Cristallo, S.; Domingo-Pardo, C.; Guerrero, C.; et al. First Measurement of the Branching  $^{79}\text{Se}(n, \gamma)$ ; Technical Report CERN-INTC-2020-065; INTC-P-580, CERN: Geneva, Switzerland, 2020.
79. Lederer-Woods, C.; Woods, P.J.; Davinson, T.; Kahl, D.; Lonsdale, S.J.; Aberle, O.; Amaducci, S.; Andrzejewski, J.; Audouin, L.; Bacak, M.; et al. Destruction of the cosmic  $\gamma$ -ray emitter  $^{26}\text{Al}$  in massive stars: Study of the key  $^{26}\text{Al}(n, p)$  reaction. *Phys. Rev. C* **2021**, *104*, L022803. [[CrossRef](#)]
80. Praena, J. Proposal to the ISOLDE and Neutron Time-of-Flight Committee: The  $^{14}\text{N}(n, p)^{14}\text{C}$  and  $^{35}\text{Cl}(n, p)^{35}\text{S}$  Reactions at n\_TOF-EAR2: Dosimetry in BNCT and Astrophysics; Technical Report CERN-INTC-2017-039; INTC-P-510, CERN: Geneva, Switzerland, 2017.
81. Ingelbrecht, C.; Moens, A.; Wagemans, J.; Denecke, B.; Altitzoglou, T.; Johnston, P. An  $^{26}\text{Al}$  target for  $(n, p)$  and  $(n, \alpha)$  cross-section measurements. *Nucl. Instrum. Methods Phys. Res. Sect. A Accel. Spectrometers Detect. Assoc. Equip.* **2002**, *480*, 114–118. [[CrossRef](#)]
82. Koehler, P.E.; Kavanagh, R.W.; Vogelaar, R.B.; Gledenov, Y.M.; Popov, Y.P.  $^{26}\text{Al}(n, p_1)$  and  $(n, \alpha_0)$  cross sections from thermal energy to 70 keV and the nucleosynthesis of  $^{26}\text{Al}$ . *Phys. Rev. C* **1997**, *56*, 1138–1143. [[CrossRef](#)]
83. Trautvetter, H.P.; Becker, H.W.; Heinemann, U.; Buchmann, L.; Rolfs, C.; Käppeler, F.; Baumann, M.; Freiesleben, H.; Lütke-Stetzcamp, H.J.; Geltenbort, P.; et al. Destruction of  $^{26}\text{Al}$  in explosive nucleosynthesis. *Z. Phys. A* **1986**, *323*, 1–11. [[CrossRef](#)]
84. Mendoza, E.; Cano-Ott, D.; Guerrero, C.; Berthoumieux, E.; n TOF Collaboration. Pulse pile-up and dead time corrections for digitized signals from a  $\text{BaF}_2$  calorimeter. *Nucl. Instrum. Methods Phys. Res. A* **2014**, *768*, 55–61. [[CrossRef](#)]
85. Schumann, D.; Dressler, R.; Maugeri, E.A.; Heinitz, S. Isotope production and target preparation for nuclear astrophysics data. *Eur. Phys. J. Web Conf.* **2017**, *146*, 03005. [[CrossRef](#)]
86. Barros, S.; Bergström, I.; Vlachoudis, V.; Weiss, C. Optimization of n\_TOF-EAR2 using FLUKA. *J. Instrum.* **2015**, *10*, P09003. [[CrossRef](#)]
87. Tagliente, G.; Milazzo, P.M.; Fujii, K.; Abbondanno, U.; Aerts, G.; Álvarez, H.; Alvarez-Velarde, F.; Andriamonje, S.; Andrzejewski, J.; Audouin, L.; et al. The  $^{93}\text{Zr}(n, \gamma)$  reaction up to 8 keV neutron energy. *Phys. Rev. C* **2013**, *87*, 014622. [[CrossRef](#)]
88. Neyskens, P.; van Eck, S.; Jorissen, A.; Goriely, S.; Siess, L.; Plez, B. The temperature and chronology of heavy-element synthesis in low-mass stars. *Nature* **2015**, *517*, 174–176. [[CrossRef](#)] [[PubMed](#)]
89. High-sensitivity Measurements of Key Stellar Nucleo-Synthesis Reactions (HYMNS), ERC-Consolidator Grant Agreement No. 681740, PI: C. Domingo Pardo. Available online: <https://cordis.europa.eu/project/id/681740> (accessed on 8 December 2021).
90. Domingo-Pardo, C. i-TED: A novel concept for high-sensitivity  $(n, \gamma)$  cross-section measurements. *Nucl. Instrum. Methods Phys. Res. A* **2016**, *825*, 78–86. [[CrossRef](#)]
91. Balibrea-Correa, J.; Leredegui-Marco, J.; Calvo, D.; Caballero, L.; Babiano, V.; Ladarescu, I.; Redondo, M.L.; Tain, J.L.; Tolosa, A.; Domingo-Pardo, C.; et al. A first prototype of  $\text{C}_6\text{D}_6$  total-energy detector with SiPM readout for neutron capture time-of-flight experiments. *Nucl. Instrum. Methods Phys. Res. A* **2021**, *985*, 164709. [[CrossRef](#)]
92. Mengoni, A. (Agenzia Nazionale per le Nuove Tecnologie (ENEA), 40129 Bologna, Italy). Personal communication, 2021.